JOURNAL OF CATALYSIS 89, 334–347 (1984)

A Surface Spectroscopic Study of Co–Mo/Al_2O_3 Catalysts Using ESCA, ISS, XRD, and Raman Spectroscopy, I[1]

LEO E. MAKOVSKY, JOHN M. STENCEL, FRED R. BROWN, RICHARD E. TISCHER, AND SIDNEY S. POLLACK

United States Department of Energy, Pittsburgh Energy Technology Center, P. O. Box 10940, Pittsburgh, Pennsylvania 15236

Received May 23, 1983; revised May 30, 1984

Laser Raman spectroscopy, X-ray photoelectron spectroscopy, low-energy ion-scattering spectroscopy, and X-ray diffraction have been used to characterize a series of Co–Mo/Al_2O_3 catalysts containing 15 wt% MoO_3 and 0 to 8 wt% CoO in their oxide, reduced, and sulfided forms. These data show that the catalyst surface contains $CoMoO_4$ and irreducible Co^{2+} ions of tetrahedral symmetry when the CoO concentration is 0 to 6%. With 7 to 8% CoO, additional surface species includes Co_3O_4 crystallites on the γ-Al_2O_3 surface. Formation of Co_3O_4 coincides with an increased Mo reducibility and a decreased BET surface area. These results are compared to previously published data on Co–Mo/Al_2O_3 and suggest that the state of dehydration–dehydroxylation of the Al_2O_3 surface before impregnation of Co and Mo affects their subsequent speciation. Autoclave studies investigating the hydrodesulfurization (HDS) and hydroconversion of coal using these catalysts are also reported. Significance of the surface speciation with respect to these activity studies is discussed.

1. INTRODUCTION

Cobalt-promoted, molybdenum catalysts, supported on alumina, are well known for their success in the hydrodesulfurization (HDS) of petroleum feedstocks and coal liquefaction products. Although no unequivocal explanation exists for the structure of the molybdena supported on alumina catalysts, many authors have described models for the interaction of molybdate ions with the alumina OH groups to form stable surface alumina–molybdic acid complexes (*1–3*). Unfortunately, the literature concerning the promoting role of cobalt in Co–Mo/Al_2O_3 catalysts is much more confusing. This literature has been summarized by Massoth (*4*) who states that the promoting role of cobalt has been ascribed to (1) an increase in Mo dispersion; (2) an increase in Mo reduction; (3) an increase in H_2 mobility; (4) an intercalation effect with MoS_2; (5) a synergism between MoS_2 and Co_9S_8 crystallites; (6) a specific kinetic effect; (7) a decrease in deactivation; (8) an increase in surface segregation of mixed sulfide phases; and (9) the prevention of MoS_2 crystallization. More recently Topsøe *et al.* (*5*) reported direct evidence of cobalt and molybdenum existing in the active form as a Co–Mo–S surface phase. All of these factors may have some influence on the HDS activity of Co–Mo/Al_2O_3.

As early as 1977, Brown *et al.* (*6, 7*), used Raman spectroscopy to identify species that exist on and in a γ-Al_2O_3 surface after impregnation with ammonium heptamolybdate and cobalt nitrate solutions. Other researchers have employed Raman spectroscopy and complimentary analytical techniques such as X-ray photoelectron spectroscopy (XPS, ESCA), ion-scattering spectroscopy (ISS), and X-ray diffraction (XRD) to identify speciation on the oxide form of this catalyst (*8–10*). These studies have shown that in CoO–MoO_3/Al_2O_3 the

[1] Reference in this report to any specific commercial product, process, or service is to facilitate understanding and does not necessarily imply its endorsement or favoring by the U.S. Department of Energy.

0021-9517/84 $3.00

following species can be identified: (1) three-dimensional compounds that include aluminum, oxygen, cobalt, and/or molybdenum, e.g., $CoMoO_4$, Co_3O_4, MoO_3, $CoAl_2O_4$, and $Al_2(MoO_4)_3$; (2) two-dimensional species that involve molybdena–alumina and cobalt–molybdenum interactions (*6, 7, 11, 12*); (3) and dispersed, ionic $Co^{\delta+}$ and $Mo^{\delta+}$ ions with coordination symmetry dependent on that available in the γ-Al_2O_3 surface (*9, 11–13*). The reducibilities of these different states are known (*9, 12, 13*) and hence, such studies have been used to exclude the existence of otherwise poorly defined species (*9, 12, 13*). However, a thorough understanding of the reasons for the generation of the aforementioned species has yet to be forwarded. It is known that the site symmetry of $Mo^{\delta+}$ is affected by calcination conditions of the impregnated catalyst and by metal concentrations (*9, 10*). Additionally, the acidity of the impregnating solutions and impregnation sequence can influence metals speciation (*14, 15*). Another factor of possible importance is the condition of the γ-Al_2O_3 support prior to metals impregnation; this factor is addressed herein.

The sulfided form of the Co–Mo/Al_2O_3 catalyst is the active form for HDS and hydroconversion of coal. Controversy still exists as to the chemical structure of the active species providing HDS and hydroconversion activity and as to the importance of the catalyst speciation in the oxide form of the catalyst that provides maximum activity upon sulfidation. A causal relationship between metals speciation or dispersion in the sulfided form of the catalyst and the HDS and hydroconversion activity has not yet been firmly established.

2. EXPERIMENTAL METHODS

2a. Instrumental

Raman spectra were recorded on a Spex Ramalog IV spectrometer equipped with holographic gratings. The exciting line for all spectra presented was the 5145-Å line from a Spectra-Physics Model No. 165 Ar^+ Laser. The laser power was varied from 25 to 45 mW in order to obtain appropriate spectra, while the spectral slit width was maintained at 4 cm^{-1}. In order to avoid decomposition due to absorption of the finely focused laser beam, the samples, ranging in color from white to blue to black, were pressed into 13-mm KBr-backed pellets and rotated with a commercial Spex rotation device. KBr offers no discrete Raman scattering; however, it does fluoresce. Since Raman spectroscopy is a scattering phenomenon and the laser beam does not completely penetrate the sample, the KBr presents no problem because it is used only to support the sample and is not mixed with the sample.

The XRD data were collected on a Rigaku horizontal goniometer. A copper X-ray tube was used and operated at 40 kV and 35 mA. Data were collected with a 1° divergent slit and a 0.3-mm receiving slit. The signal was analyzed with a receiving graphite monochromator and scintillation counter with a pulse-height discriminator. The samples were ground and packed into a glass-plate holder with an opening 20 × 16 × 0.5 mm, and no binder was used.

The ISS analyses were performed with a 3M SIMS/ISS spectrometer and data processor. The data were collected with a rastered, primary $^4He^+$ beam voltage of 1500 eV, and the signal was analyzed with a cylindrical mirror analyzer. Data were collected at intervals of 0–10, 10–20, and 20–40 min. A baseline pressure of 1×10^{-9} Torr was maintained for the ISS, however to obtain spectra, the vacuum system was backfilled with ^4He to a pressure of 5×10^{-5} Torr. In order to assure a representative surface, data are reported for the 10- to 20-min sputter and data collection interval. The peak intensity of Co or Mo is presented as a ratio to the intensity of Al. The powdered samples were pressed into 13-mm pellets with no binder and supported on the 3M stainless-steel sample holder to facilitate data acquisition.

A McPherson ESCA 36 was used to collect data on the oxide catalyst and an AIE ES 200 electron spectrometer was used to collect data on the reduced and sulfided catalysts. Baseline vacuums of 1×10^{-8} Torr for the McPherson and 1×10^{-9} Torr for the AEI were obtained. The X-ray source was a Mg anode operated at 10 to 22 mA and 15 kV. The oxide forms of the catalysts were mounted in the spectrometer by scraping the powdered samples across etched aluminum plates and then supporting the plates within the vacuum chamber. For reduced or sulfided samples, thin wafers of the catalysts were mounted on a reaction transfer probe which was then alternately used in a reaction furnace and in the transfer of samples to the vacuum chamber of the spectrometer. This probe and reaction furnace have been described (*9, 16*). The Al 2*p* line at 74.5 eV of the Al_2O_3 support was used as an internal standard for correction of binding energies. The ESCA data is presented as intensity ratios of Mo/Al and Co/Al.

2b. Catalyst Preparation

To investigate effects of variation in Co concentration, a set of samples was prepared in which the concentration of molybdenum was held constant at 15 wt% (all concentrations will be expressed as the wt% oxide of the metal), and the concentration of cobalt incrementally increased from 0 through 8 wt%. The nominal concentrations of Co and Mo are in good agreement with the concentrations as determined by atomic absorption. Hence, for the sake of convenience, the nominal concentrations will be used in all of the following sections. This set of samples will be labeled as (0–8) CoO–15 MoO_3/Al_2O_3. Commercial HDS catalysts usually contain about 3 wt% cobalt (calculated as CoO), 15 wt% molybdenum (calculated as MoO_3), and 82 wt% Al_2O_3. The maximum effect on activity as a result of a promoter such as Co has been found by Delmon (*17*) to be for an atomic proportion r = (Group VIII metal)/(Group VIA + Group VIII metal) between the approximate values of 0.15 and 0.50. The value r for catalysts discussed herein varies from 0.11 to 0.51.

The Al_2O_3 support was a Harshaw 4104 E alumina that had a BET surface area of 210 m^2/g and an average port diameter of 115 Å. Our analyses showed $\leq 0.095\%$ for both sodium and calcium and the manufacturer's chemical analysis (500°C basis) showed less than 0.001% of iron, magnesium, and silicon. The 1/32-in. extrudates were ground to −100 mesh and calcined at 500°C for 1 h prior to Mo and Co impregnation. The Al_2O_3 was molybdenum impregnated to incipient wetness with an aqueous solution of ammonium heptamolybdate, dried at 120°C, impregnated with aqueous solution of cobalt nitrate, dried at 120°C, and finally recalcined at 500°C for 16 h. Confusion concerning the XRD patterns of γ- and η-Al_2O_3 is the result of subtle differences in XRD patterns (*18*). The 4104 E alumina is marketed as γ-Al_2O_3 and will be described as such in the remainder of this paper.

2c. Activity Measurements

Batch autoclave tests were carried out in a 1-liter Autoclave Engineers' Magnadrive autoclave equipped with a 2-liter hydrogen reservoir. The charge consisted of 75 g of coal (moisture-free), 75 g of Panasol AN-3 (commercially available aromatic product consisting of mono, di-, and trimethyl naphthalenes), and 2.812 g of presulfided catalyst. The unit was pressurized with hydrogen gas to 68.9–75.8 bar and heated to 430°C, which required approximately 45 min. During this time the pressure increased to 137.8 bar. The hydrogen reservoir was then opened, which maintained the reactor at 137.8 bar during a 30-min reaction period. At the end of the reaction period, the autoclave was isolated from the reservoir and quenched to room temperature by means of an internal cooling coil and external air cooler.

The work-up procedure for the activity samples consisted of recovering approximately 90–95% of the product, homogeniz-

ing the recovered portion, and obtaining aliquot samples. Conversions based on the product solubility in three different solvents were determined using a modified version of a microfiltration procedure (*19*). Values were obtained for conversion of the coal to tetrahydrofuran solubles, to ethyl acetate solubles, and to pentane solubles. The conversion of coal to preasphaltenes, asphaltenes, and oil can be derived from this data. The product not used for the conversion determinations was centrifuged at 10,000 rpm in a Sorvell Model RC-5 Superspeed centrifuge, and a sulfur analysis of this product was obtained by X-ray fluorescence using a calibration based on NBS and LECO sulfur standards. The method has a precision of ±0.03% and an accuracy of ±0.1%.

3. EXPERIMENTAL RESULTS

3a. Oxide Catalyst Studies

Representative Raman spectra of the (0–8) CoO–15 MoO_3/Al_2O_3 catalysts are shown in Fig. 1. The spectrum of the baseline catalyst (0 wt% CoO and 15 wt% MoO_3) in Fig. 1a has been previously interpreted (*6, 7*) as showing the molybdenum–alumina interaction species. The catalysts prepared with the addition of up to 2 wt% CoO yield essentially the same spectrum, i.e., no species indicative of the presence of cobalt, either noninteracting, interacting with molybdenum, or interacting with the alumina support. However, closer examination of the Raman data shows the bandwidth increases from 50 to 70 cm^{-1} for 0 to 2% CoO concentrations. This bandwidth increase is the result of a Raman band at 938 cm^{-1}, which is clearly evident in Fig. 2 (an expanded view of the 950-cm^{-1} region) and which is increasing in intensity as the CoO concentration increases. The bandwidth decreases to 20 cm^{-1} at the 4% Co loading and at the 8% Co loading the bandwidth is approximately 15 cm^{-1}. This decrease in bandwidth at 3 wt% CoO and above is associated with enhancement of the narrow 938-

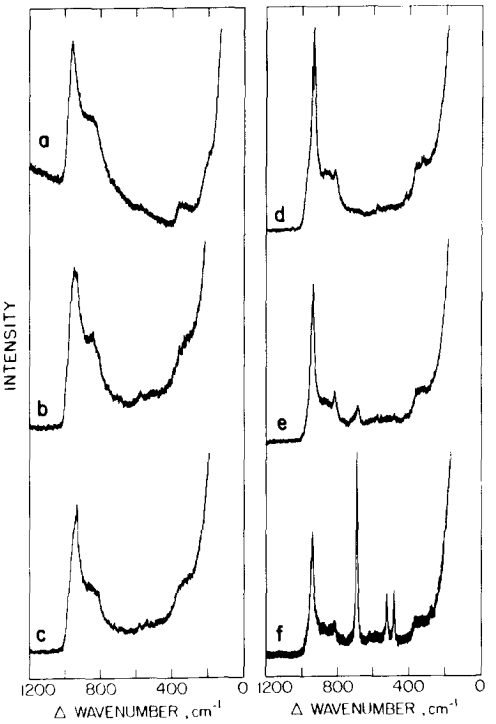

FIG. 1. Raman spectra of (a) 0% CoO–15% MoO_3/Al_2O_3, (b) 2% CoO–15% MoO_3/Al_2O_3, (c) 3% CoO–15% MoO_3/Al_2O_3, (d) 4% CoO–15% MoO_3/Al_2O_3, (e) 7% CoO–15% MoO_3/Al_2O_3, (f) 8% CoO–15% MoO_3/Al_2O_3.

cm^{-1} band relative to the 950-cm^{-1} interaction species band. Comparison of the 938-cm^{-1} band frequency with that from standard reference compounds (Fig. 3c) and with the Raman results at higher CoO loadings shows the existence of $CoMoO_4$ at loadings as low as 3 wt% CoO. By similar comparisons, it is also evident that with 8 wt% CoO the catalyst contains Co_3O_4 species.

The effects of the thermal history of the alumina were investigated by preheating the alumina at 120, 300, 400, 500, 700, and 900°C before impregnating to a loading of 15% MoO_3 and 3% Co. The Raman spectra (Fig. 4), show that as the pretreatment temperature increases, the 950-cm^{-1} band changes shape on the low-frequency side, especially at the 500°C pretreatment and above. At 700°C and particularly 900°C, the 938-cm^{-1} peak of $CoMoO_4$ is evident. The

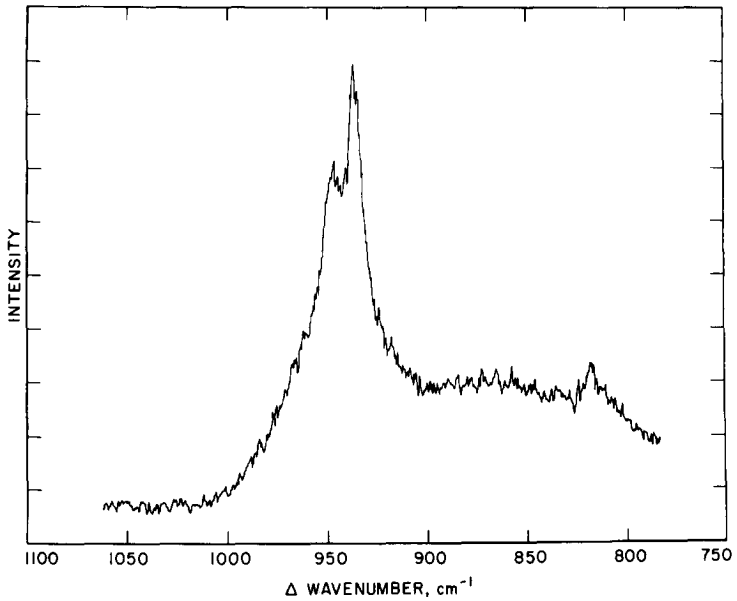

FIG. 2. Expanded wavenumber scale of the 950-cm^{-1} Raman region for the 4% CoO–15% MoO_3/Al_2O_3.

presence of $CoMoO_4$ was confirmed by X-ray diffraction data shown in Fig. 5. The most intense line of $CoMoO_4$ at 26.5 degrees 2θ is particularly evident at the 500°C precalcination temperature and above.

The XRD results for the (0–8) CoO–15 MoO_3/Al_2O_3 catalysts confirm the Raman findings and are summarized in Table 1. The baseline catalyst does not contain cobalt; however, it does contain 15 wt%

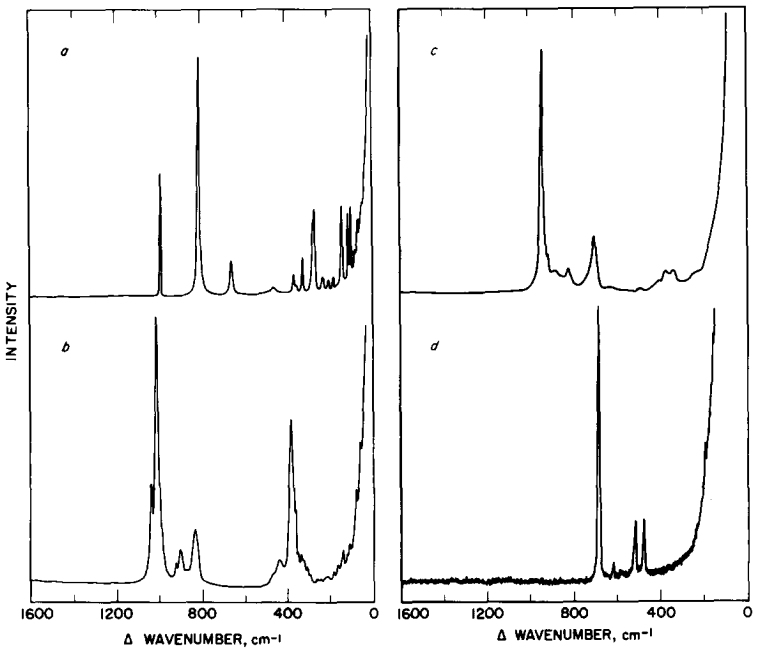

FIG. 3. Raman spectra of (a) MoO_3, (b) $Al_2(MoO_4)_3$, (c) $CoMoO_4$, and (d) Co_3O_4.

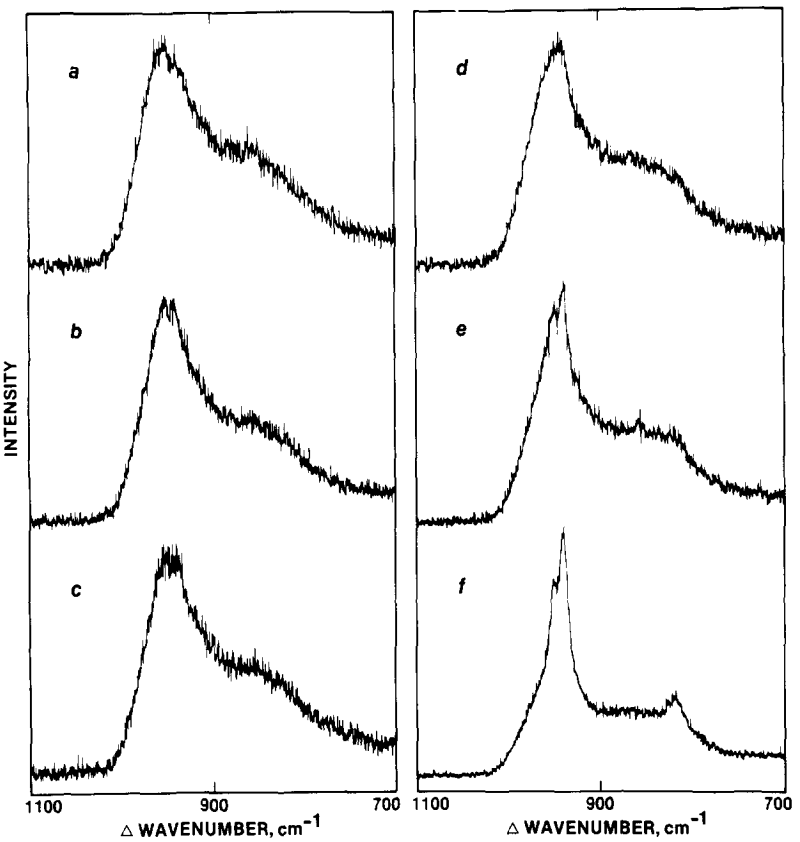

FIG. 4. Raman spectra of 3% CoO–15% MoO_3/Al_2O_3 catalysts which have been prepared on Al_2O_3 which has been preheated to (a) 120°C, (b) 300°C, (c) 400°C, (d) 500°C, (e) 700°C, and (f) 900°C immediately before preparation.

MoO_3, which is not discernible from the XRD results. The strongest diffraction line for $CoMoO_4$ is present for CoO concentrations as low as 2%, and the diffraction pattern for $CoMoO_4$ becomes stronger as the CoO concentration is increased. At approximately 5 wt% CoO, $CoMoO_4$ is a major contributor to the diffraction pattern of the catalyst.

The ISS results for the (0–8) CoO–15 MoO_3/Al_2O_3 catalysts are summarized in Fig. 6. This figure shows that the Co/Al intensity ratio, hereafter referred to as the Co ratio, increases slightly to about 3% CoO loading, levels off, and then becomes nearly constant. The Mo/Al ratio, hereafter denoted by the Mo ratio, decreases with increasing CoO concentration up to approximately 5% CoO loading, and then is nearly constant. Confidence in the ISS data was gained by obtaining spectra from a set of synthetic (0–8) CoO–15 MoO_3/Al_2O_3 samples that were prepared by physically mixing Co_3O_4, MoO_3, and Al_2O_3. A plot of this data, not shown, indicates that as the wt% Co is increased in these samples, the Co/Al + Mo + Co ratio is linear and has a positive slope. The Mo/Al + Mo + Co ratio is also linear; however, the slope is approximately zero. The Al/Al + Mo + Co ratio is also linear; however, the slope is negative. These results were anticipated because as the percentage of CoO is increased, the percentage of Al_2O_3 decreases.

The ESCA ratios plotted as a function of the wt% CoO for the (0–8) CoO–15 MoO_3/Al_2O_3 catalysts are shown in Fig. 7. The Mo ratios slowly decrease to a loading of 6%

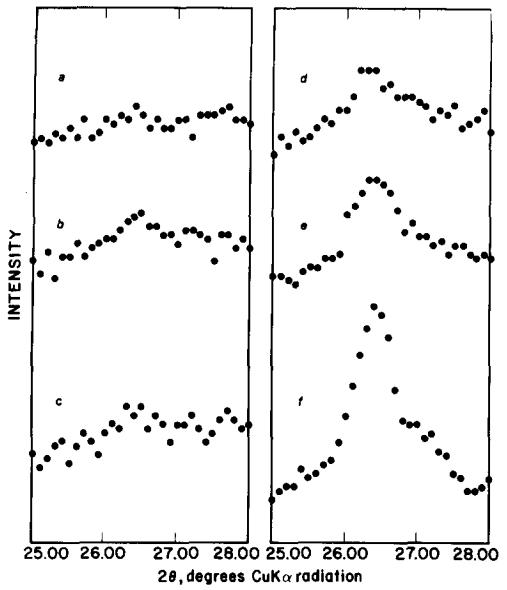

FIG. 5. X-Ray diffraction patterns of the 26.5 degrees 2θ line of 3% CoO–15% MoO_3/Al_2O_3 catalysts which have been prepared on Al_2O_3 which has been preheated to (a) 120°C, (b) 300°C, (c) 400°C, (d) 500°C, (e) 700°C, and (f) 900°C immediately before preparation.

CoO, after which it increases dramatically. The Co ratio also increases dramatically with an increase in the CoO loading from 5 to 8% CoO. In terms of the analysis of bandshapes of the oxide form of these catalysts, it has been shown that spin-orbit splittings of the Co $2p_{3/2}$ and $2p_{1/2}$ levels (Δ_{Co}), and the difference between the $2p_{3/2}$

TABLE 1

X-Ray Diffraction Results of both the Major Components and Minor Components of the (0–8) CoO–15 MoO_3/Al_2O_3 Catalysts

wt% CoO	Major component	Minor component
0	Al_2O_3	
1	Al_2O_3	
2	Al_2O_3	$CoMoO_4$ (strongest line)
3	Al_2O_3	$CoMoO_4$
4	Al_2O_3	$CoMoO_4$
5	Al_2O_3, $CoMoO_4$	
6	Al_2O_3, $CoMoO_4$	
7	Al_2O_3, $CoMoO_4$	
8	Al_2O_3, $CoMoO_4$	Co_3O_4

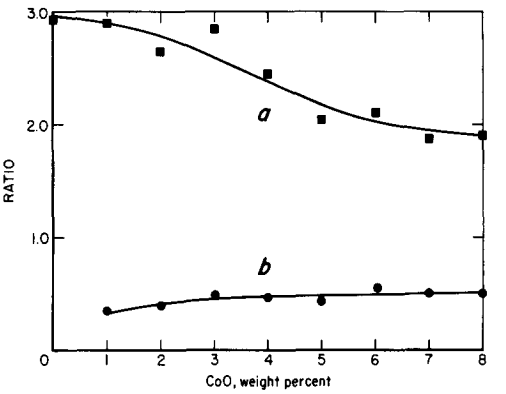

FIG. 6. Plot of ISS ratios as a function of CoO concentration for the (0–8)% Co–15% MoO_3/Al_2O_3 catalysts. The data was collected after 10 and 20 min into the scan. The plot shows (a) Mo/Al and (b) Co/Al intensity ratios.

level and a satellite at approximately 5–6 eV higher binding energy (Δ_S) can provide information on the oxidation state and coordination of the Co (*20–22*). The chemical state of Co cannot be determined by using only the ESCA Co binding energy values (*22*). With 1 to 3% CoO, the value of Δ_{Co} is 16.1 ± 0.2 eV and Δ_S is 5.0 ± 0.2 eV. In the 4 to 7% CoO catalysts, Δ_{Co} is constant at 16.0 eV, with Δ_S averaging 5.7 eV. At 8% CoO, Δ_{Co} is 15.6 eV and Δ_S is 5.1 eV. These results suggest paramagnetic cobaltous

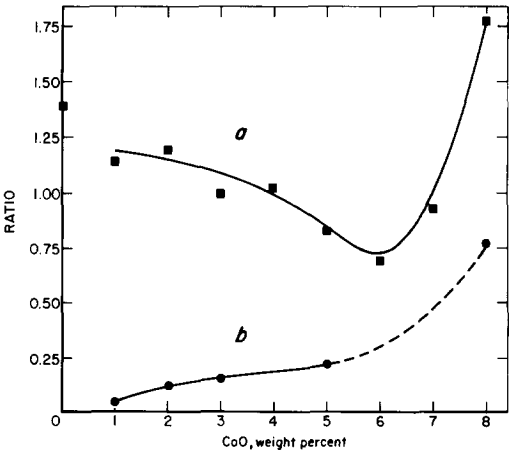

FIG. 7. Plot of ESCA ratios as a function of CoO concentration for the (0–8)% CoO–15% MoO_3/Al_2O_3 catalysts in the oxide form. (a) Mo/Al and (b) Co/Al intensity ratios.

(Co^{2+}) with tetrahedral coordination with 1 to 3% CoO, octahedral coordination of Co with 4 to 7% CoO, and a mixture of Co^{2+} and diamagnetic Co^{3+} with a different coordination at 8% CoO. Such conclusions are in agreement with the XRD and Raman results showing $CoMoO_4$ and Co_3O_4 at the various CoO loadings.

3b. Reduced and Sulfided Catalyst Studies

Table 2 lists the binding energies of the (0–8) CoO–15 MoO_3/Al_2O_3 catalysts after having been reduced in flowing H_2 at 500°C for 5 h. Figure 8 shows the spectra of the Co $2p_{3/2}$ and Mo $3d_{5/2,3/2}$ levels after this H_2 reduction with a reference line drawn through the positions of the peaks listed in Table 2. From the spectra of the Co $2p_{3/2}$ levels, an estimation of the percentage of CoO reducible to metallic Co can be obtained; these values are listed in Table 3. The constant percentage of reducible CoO for the catalysts containing from 1 to 3% CoO shows that the absolute amount of CoO detected by ESCA to be reducible to Co metal increases from approximately 0.4 to 1 wt% in these three catalysts. At a 5% CoO loading the amount of Co metal after reduction is nearly 2 wt%, while at an 8% CoO loading approximately 5.6 wt% of the CoO is observed to be reducible. These values are three times larger than those reported by Chin and Hercules (*13*) for CoO–MoO_3/Al_2O_3 having identical metal loadings. Reasons for this difference will be discussed in the following section.

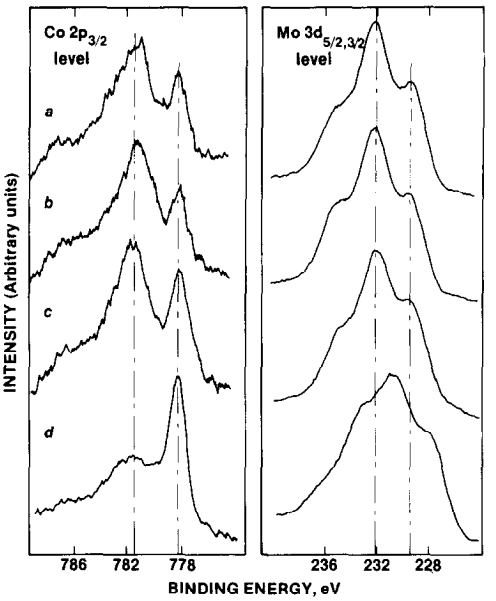

FIG. 8. The ESCA spectra of Co $2p$ and Mo $3d_{5/2,3/2}$ levels after 500°C, H_2 reduction of the (0–8)% CoO–15% MoO_3/Al_2O_3 catalysts at (a) 2, (b) 3, (c) 5, and (d) 8% CoO loadings.

The reference line at ca. 229.3 eV in the Mo $3d_{5/2,3/2}$ spectra in Figs. 8a, b, and c is in agreement with the position of Mo^{4+} (*9*, *13*); the shape of these Mo bands also indicates the presence of Mo^{5+}. However, with an 8% CoO loading (Fig. 8d) a band appears near 227 eV, a position in agreement with that for Mo metal. Since Co_3O_4 and

TABLE 2

Binding Energies of Co $2p$ and Mo $3d$ Levels in 500°C, H_2-Reduced (0–8) CoO–15 MoO_3/Al_2O_3 Catalysts

% CoO	BE, eV			
	Co $2p_{3/2}$		Mo $3d_{5/2}$	Mo $3d_{3/2}$
0			229.2	232.1
1	778.0	781.4	229.5	232.2
2	778.1	781.5	229.4	232.2
3	778.1	781.2	229.4	232.1
5	777.9	781.4	229.6	232.2
8	777.7	781.4	(227)[a]	

[a] See Text and Figure 8d.

TABLE 3

Percentage of the CoO in (0–8) CoO–15 MoO_3/Al_2O_3 that is Reducible to Co Metal Using H_2 at 500°C for 5 h

wt% CoO	% Reduction
1	36
2	34
3	36
5	42
8	74

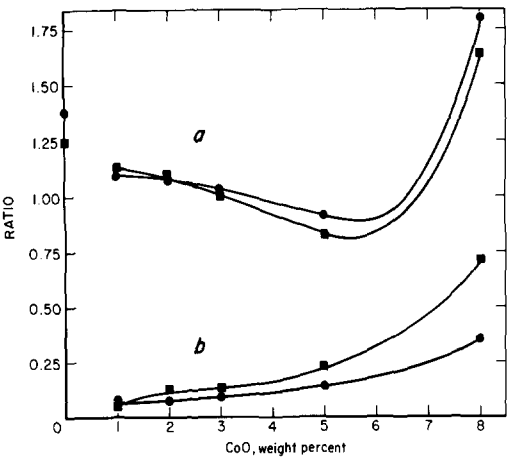

FIG. 9. Plot of ESCA ratios as a function of CoO concentration for (a) 500°C, H_2-reduced catalysts, and for (b) 250°C, 10% H_2S/H_2-sulfided catalysts.

$CoMoO_4$ contain cobalt reducible to Co metal, and $CoMoO_4$ contains molybdenum reducible to Mo metal, the reducibility of the 8% CoO sample agrees with those reducibilities expected from the characterization of the oxidic form of the catalyst.

The Mo and Co ratios obtained from ESCA studies of reduced and sulfided catalysts are shown in Fig. 9. A minimum in the Mo ratio appears near 5% CoO, and both the Mo and Co ratios exhibit large increases in the 5 to 8% CoO range; this behavior is similar to that shown in Fig. 7. The ESCA spectra of the Co $2p_{3/2}$ and Mo $3d_{5/2,3/2}$ levels of these catalysts after sulfidation in 15% H_2S/H_2 at 250°C for 1 h are shown in Figs. 10 and 11, respectively. Corresponding binding energies are listed in Table 4. These spectra and binding energies are similar to those reported by Chin and Hercules (*13*)

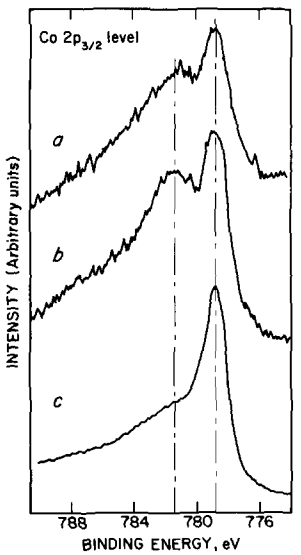

FIG. 10. The ESCA spectra of the Co $2p_{3/2}$ level in (0–8)% CoO–15% Mo/Al_2O_3 catalysts sulfided at 250°C for 1 h in 10% H_2S/H_2 at (a) 2, (b) 5, and (c) 8% CoO loadings.

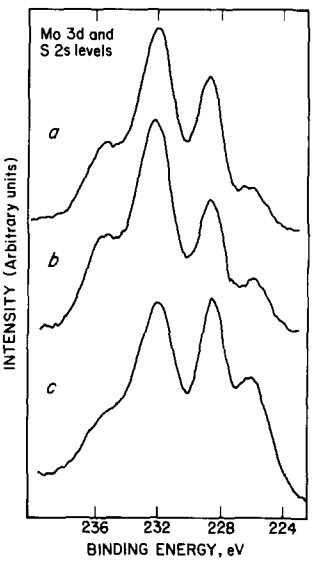

FIG. 11.The ESCA spectra of the Mo $3d_{5/2,3/2}$ levels in (0–8)% CoO–15% MoO_3/Al_2O_3 catalysts sulfided at 250°C for 1 h in 10% H_2S/H_2 at a (a) 2, (b) 5, and (c) 8% CoO loadings.

TABLE 4

Binding Energies of Co 2*p* and Mo 3*d* Levels in 250°C, 10% H_2S/H_2 Sulfided, (0–8) CoO–15 MoO_3/Al_2O_3 Catalysts

% CoO	BE, eV				S 2p
	Co $2p_{3/2}$		Mo $3d_{5/2}$	Mo $3d_{3/2}$	
0			228.7	232.8	162.1
1	778.6	781.6	228.7	232.1	162.1
2	778.7	781.4	228.7	232.0	162.1
3	778.7	781.5	228.8	232.3	162.1
5	778.5	781.7	228.6	232.3	162.1
8	778.7		228.4	231.8	161.9

except that in all cases the intensity of the Co 2*p* peak at ca. 778 eV relative to the peak at ca. 781.5 is larger for the catalysts discussed herein than for those catalysts discussed in (*13*).

The (0–8) CoO–15 MoO_3/Al_2O_3 series was investigated for activity with respect to both sulfur removal and conversion of coal to liquid products. From the combination of results from sulfur analyses of the centrifuged coal liquids, sulfur analyses of the original coal and solvent, and a sulfur-type analysis of the original coal, the amount of organic sulfur removed during liquefaction can be calculated as percentages and plotted as a function of wt% CoO, as shown in Fig. 12. These results show removal of at least an additional 22% of the product sulfur compared to a corresponding experimental thermal (noncatalytic) run, which removes 58.2 ± 0.6% sulfur. In Table 5, the percentage conversion of coal to THF, ethyl acetate, and pentane solubles is shown, along with the corresponding thermal conversions. The conversions are substantially higher in the catalyzed runs than in the thermal run. However, no significant changes in conversion were noted with respect to the wt% CoO in the catalysts.

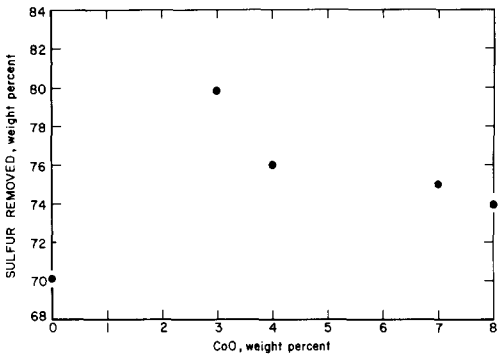

FIG. 12. Percentage of sulfur removed as a function of CoO concentration.

4. DISCUSSION

The Raman and the XRD characterization data agree that $CoMoO_4$ is formed after the addition of 2% CoO, and that Co_3O_4 is present at 8% CoO. The BET surface areas were also acquired for these catalysts. For 0 CoO–15 MoO_3/Al_2O_3, the surface area was 184 $m^2/(g\ Al_2O_3)$, a value 12% below the value obtained for γ-Al_2O_3. With further addition of CoO and the formation of $CoMoO_4$, the BET surface area was not significantly altered from this approximate 180-m^2/g value. However, the formation of Co_3O_4 in the 7 to 8% CoO range accompanies a decreased surface area of an additional 10% to approximately 160 $m^2/(g\ Al_2O_3)$. A monolayer surface species should not decrease the surface area, whereas three-dimensional crystallites which are large enough to be detected by XRD (ap-

TABLE 5

Activity as % Conversion and % Organic Sulfur Removed as a Function of % CoO for Catalysts Containing 15% MoO_3

	Thermal	wt% CoO in catalyst					
		0	2	3	4	7	8
a. % Conversion							
THF	80.5 ± 0.4	94.1	93.6	94.1	95.0	94.3	99.3
Ethyl acetate	60.5 ± 0.7	80.4	80.6	85.8	83.9	N.A	86.7
Pentane	30.4 ± 0.3	41.0	39.5	39.2	41.3	37.3	44.8
b. % Organic sulfur removal	58.2 ± 0.6	70.1	N.A	79.8	76.0	75.0	73.8

Note. Activity determined at 430°C, 2000 psi, 30-min reaction time, and 3.75 wt% catalyst loading using a 1/1 mixture of Illinois No. 6 Burning Star Mine Coal and Panasol AN solvent. Catalyst presulfided for 4 h in 10% H_2S in hydrogen at 350°C.

proximately 50 Å) and in direct contact with the Al_2O_3 should decrease the surface area of the Al_2O_3. Hence, the 0 CoO–15 MoO_3/Al_2O_3 catalyst may contain three-dimensional molybdena species other than just the molybdate, monolayer interaction species shown to exist in the Raman spectrum (Fig. 1a). The ESCA spectrum of the Mo 3*d* levels for the 0 CoO–15 MoO_3/Al_2O_3 catalyst and its Mo reducibility suggest that not all of the Mo is in a monolayer form. After reduction the Mo(VI) in this catalyst became a mixture of Mo(IV) and Mo(V) in the approximate ratio 75 : 25. This Mo(IV) : Mo(V) ratio is larger than that reported by Zingg *et al.* (*9*) for their Mo/Al_2O_3 preparation and is larger than the Mo(IV) : Mo(V) ratio once Co was present in similar Co–Mo/Al_2O_3 catalysts (*13*). If the ratio of tetrahedral-to-octahedral surface sites in noncalcined 200 m^2/g γ-Al_2O_3 is 2 : 1 (*23*), and if tetrahedral sites are filled first with subsequent filling of the octahedral sites to a monolayer coverage of ~20% MoO_3 (*9, 24, 25*), then the 75 : 25 Mo(IV) : Mo(V) ratio in the reduced 15% MoO_3/Al_2O_3 catalyst may signify an alteration of the Al_2O_3 surface for catalysts studied herein as compared to that found in noncalcined Al_2O_3 (*9, 13, 23*). As a consequence of this alteration, the interaction between the Mo and the Al_2O_3 surface may differ and the uniformity of the Mo monolayer may decrease from that previously reported (*13*).

The Mo ratios in Figs. 6 and 7 for the 2 to 6% CoO-containing catalysts decrease as the intensities of $CoMoO_4$ peaks increase in the Raman and XRD data. Such behavior can be expected during growth in the size of the three-dimensional $CoMoO_4$ crystallites or during an increase in the concentration of $CoMoO_4$ crystallites. These two possibilities cannot be separated in the present studies. However, an increase in $CoMoO_4$ intensities portends a decrease in the coverage of the Al_2O_3 by any Mo monolayer species. Such an occurrence is indicated by the relative decrease in intensity of the characteristic, broad Raman band of the Mo monolayer species near 950 cm^{-1} in Fig. 1, and its replacement with a narrow 938-cm^{-1} band due to $CoMoO_4$. During this scavenging of the Mo monolayer, the Al_2O_3 surface is gradually uncovered. Hence, a decreasing Mo ratio in Figs. 6 and 7 is in part a result of an increasing Al signal. In addition, XRD detection of $CoMoO_4$ relies on a minimum crystallite size of approximately 50 Å, a dimension larger than the ISS and ESCA sampling depths. Thus, another factor causing a decrease in the Mo ratios is the inability of ISS and ESCA to detect all of the Mo when $CoMoO_4$ is present.

With 6 to 8% CoO, the Co and Mo ratios from the ESCA studies in Fig. 7 increase whereas those from the ISS studies in Fig. 6 level to constant values. This behavior, in conjunction with the known formation of Co_3O_4 in this CoO concentration region, suggests that the Co_3O_4 does not form on top of the $CoMoO_4$ crystallites since such a location would necessitate a decrease in the Mo ratio as Co_3O_4 shields $CoMoO_4$ from detection. As a consequence of Co_3O_4 formation on the Al_2O_3 surface, some Al would be shielded from ESCA detection causing the Mo/Al and Co/Al ratios to increase, and the BET surface area would decrease. Hence, the (2–6) CoO–15 MoO_3/Al_2O_3 catalysts contain a residual Mo monolayer and $CoMoO_4$ crystallites associated with Mo multilayers. In the 8 CoO–15 MoO_3/Al_2O_3 catalyst, Co_3O_4 is also present and is associated with the Al_2O_3. However, such structure does not adequately explain the difference in behavior of the ISS and ESCA obtained Mo and Co ratios in the 7 to 8% CoO concentration region (Figs. 6 and 7) nor the large increase in reducibility of the molybdenum at a 8% CoO loading (compare Figs. 8c and d). Possibly, the difference in ISS and ESCA sampling depths or interactions between Co_3O_4 and $CoMoO_4$ which facilitate transfer of hydrogen to reduce the molybdenum may be important factors for explanation of this behavior. The behavior of the ESCA obtained Mo and Co ratios is the same in the oxide, reduced,

and sulfided forms of the catalysts; this fact shows that the speciation in the oxide precursors determines the speciation and crystallite size in the sulfided, active form of these catalysts.

It is realized that $CoMoO_4$ may not be generally found in commercial Co–Mo/Al_2O_3 catalysts containing 3% CoO and 15% MoO_3 (*26*). Medema *et al.* (*8*) have shown that $CoMoO_4$ is formed after the concentration of Mo (25 wt%) and Co (8.3 wt%) is above the concentration needed for monolayer coverage. The Raman and XRD results of 3 CoO–15 MoO_3/Al_2O_3 catalysts show that higher precalcination temperatures of Al_2O_3 before metals impregnation increase the formation of $CoMoO_4$.

During Mo impregnation onto Al_2O_3, it is generally believed that the state of the Mo is controlled by the interaction of Mo with surface hydroxyl groups (*27*). Dehydroxylation of Al_2O_3 at high temperatures leads to a decrease in OH-density and an increase in oxygen atom and anion vacancy density (*23*). A 100°C drying of Al_2O_3 before Mo impregnation would not cause significant dehydroxylation whereas at 500°C the Al_2O_3 may be 50% to 75% dehydroxylated (*23*). We are unable to comment on the manufacturer's calcination procedures. Rehydroxylation and rehydration will occur during exposure of the Al_2O_3 to ambient conditions, particularly with aqueous impregnations. However, some nonreversible reordering of the OH groups and their densities could occur as a result of 500°C and higher treatment (*28, 29*). Hence, with such changes the interaction of the Mo with the surface of the Al_2O_3 may be decreased to the extent that at a 15% MoO_3 loading not all of the Mo is firmly fixed to the surface. Thereby, the possibility of Co–Mo interactions that would initiate $CoMoO_4$ formation may be increased. The XRD data shows the presence of δ-Al_2O_3 only for the sample precalcined at 900°C. The most intense line of $CoMoO_4$ at 26.5° 2θ in Fig. 5 increases in a regular manner from 500 to 700°C, through 900°C pretreatment without being affected by the presence of δ-Al_2O_3. Further investigations concerning the relationship between nonreversible dehydroxylation and $CoMoO_4$ formation are warranted.

That cobalt sulfide is formed after H_2S treatment of the catalysts is indicated in Fig. 10 by the increased intensity of the peak at 778.5 eV relative to the intensity of the same peak for the reduced catalysts in Fig. 8. Similarly, the cobalt sulfide formation is signified by the increasing S/Mo intensity ratio with increasing CoO concentration and constant MoO_3 concentration. These results are in agreement with those from the study by Chin *et al.* (*13*). Also, the Mo $3d_{5/2,3/2}$ spectra in Fig. 11 show that with up to a loading of 5% CoO the Co has no effect on the Mo sulfidation as determined by the similar bandshapes and binding energies; this effect has also been noted by Chin *et al.* (*13*). However, at an 8% CoO concentration it is clear that the extent of Mo sulfidation has increased as indicated by the increased relative intensity of the S_{2s} peak at approximately 226 eV. This increase parallels the increased reducibility of the Mo shown in Fig. 8.

Batch autoclave screening tests measure the initial activity of the catalysts. The conversion obtained during a liquefaction test depends on the choice of coal, solvent, and reaction conditions. Conversion of coal during such a test can occur due to thermal reactions and/or catalytic reactions due to activity of the mineral matter associated with the coal. The reaction temperature was chosen from state of the art techniques to minimize the thermal reactions and emphasize the catalytic reactions. Illinois No. 6-Burning Star Mine Coal has been used as a standard coal in such tests (*34, 35*). The solvent, Panasol AN-3, is originally present in a hydrogen deficient form, which makes the test in part a measure of the activity of the liquefaction catalyst to hydrogenate the solvent under liquefaction conditions, which may be one of the principle functions of the liquefaction catalyst. Direct hydrogenation of coal liquids also occurs. The ab-

sence of any change in the percentage conversion of coal to products soluble in THF, ethyl acetate, and pentane solubles with a change in CoO concentration is not well understood, in view of the nature of the test. The test can detect differences in activity between some liquefaction catalysts, but the differences tend to be small because of thermal and hydrogen donor effects present in the reaction systems. Also, autoclave tests provide only initial activity measurements, while the differences in Co–Mo/Al_2O_3 liquefaction catalysts occur mainly in deactivation tests. These data were not obtained because of the expense and time necessary for such continuous-life tests. As can be seen in Table 5, the conversion of coal to products soluble in THF and ethyl acetate involves a very large thermal component that will tend to mask catalytic effects. If the thermal effects are subtracted from the results, the 3% CoO catalyst shows an additional 22% contribution to HDS activity, which is quite respectible. Conversion of coal to pentane-soluble products provides a better indication of catalyst performance. Again, continuous flow tests would be required to determine if the absence of any change in pentane conversion denotes the absence of a cobalt promoting effect on hydrogenation activity in these catalysts, or if it is caused by poor gas/slurry contact in our batch test. In general, HDS activity of Mo/Al_2O_3 is comparable to that found for Co–Mo/Al_2O_3, although the latter catalyst can maintain its HDS activity for longer periods. It is believed that the Mo is associated with desulfurization, while Co provides synergistic effects in both unsupported and supported systems (*30–33*). Such a synergistic effect may be indicated by the 10% increase in removed sulfur for the 3% CoO containing catalyst versus that for the 0% CoO sample (Fig. 12). The cobalt associated with the surface of the catalysts at 1 to 3% CoO loadings is well-dispersed and has constant reduction and sulfidation characteristics. These results suggest that this surface may closely approximate a Co–Mo–S phase in the sulfided state of the catalyst, thereby providing the promotion-synergistic effects as indicated by Topsøe *et al.* (*5*). If the thermal effects are subtracted from the results, the maximum catalytic contribution to HDS activity is lower but in line with those of Wivel *et al.* (*36*). The lower activity demonstrated by our data could be due to the high overall conversion and catalyst deactivation created by using coal.

5. CONCLUSIONS

It has been shown that $CoMoO_4$ can be formed on γ-Al_2O_3 during sequential Mo and Co impregnation at the expense of the Mo–Al_2O_3 interaction species. The $CoMoO_4$ formation has been associated with an alteration in the Al_2O_3 surface resulting from a 500°C drying before Mo impregnation. After an approximate 85% depletion of the Mo–Al_2O_3 interaction species, Co_3O_4 is formed and the BET surface area decreases. Desulfurization activity for these catalysts is maximized in the CoO concentration range similar to that found for commercial Co–Mo/Al_2O_3 preparations. Conversion activity shows insignificant changes. Higher precalcination of the Al_2O_3 support before metals impregnation has been shown to promote the presence of $CoMoO_4$.

ACKNOWLEDGMENTS

This research was supported by the U.S. Department of Energy through funding from the Office of Basic Energy Sciences. The authors gratefully acknowledge Catherine McCluskey, a participant in the ORAU Professional Internship Program, for assistance with the surface area measurements and to Raymond A. Hahn at the Pittsburgh Energy Technology Center for obtaining the atomic absorption data. Special thanks are also due David Hercules, Marwan Houalla, and Brian Strohmeier at the University of Pittsburgh for enlightening discussions.

REFERENCES

1. Massoth, F. E., *J. Catal.* **30,** 204 (1973).
2. Giordano, N., Bart, J. C. J., Vaghi, A., Castellan, A., and Martinotti, G., *J. Catal.* **36,** 81 (1975).

3. Fransen, R., Van Der Meer, O., and Mars, P., *J. Catal.* **42,** 79 (1975).
4. Massoth, F. E., "Advances in Catalysis," Vol. 27, p. 265. Academic Press, New York, 1978.
5. Topsøe, H., Clausen, B. S., Candia, R., Wivel, C., and Mørup, S., *J. Catal.* **68,** 433 (1981).
6. Brown, F. R., Makovsky, L. E., and Rhee, K. H., *J. Catal.* **50,** 162 (1977).
7. Brown, F. R., Tischer, R. E., Makovsky, L. E., and Rhee, K. H., "Preprint, The Division of Petroleum Chemistry, Inc., American Chemical Society, Anaheim Meeting. March 12–17, 1978."
8. Medema, J., van Stam, C., de Beer, V. H. J., Konings, A. J. A., and Koningsberger, D. C., *J. Catal.* **53,** 386 (1978).
9. Zingg, D. S., Makovsky, L. E., Tischer, R. E., Brown, F. R., and Hercules, D. M., *J. Phys. Chem.* **84,** 2898 (1980).
10. LoJacono, M., Cimino, A., and Schuit, G. C. A., *Gazz. Chim. Ital.* **103,** 1281 (1973).
11. Gajardo, P., Grange, P., and Delmon, B., *J. Catal.* **63,** 201 (1980).
12. Chin, R. L., and Hercules, D. M., *J. Phys. Chem.* **86,** 360 (1982).
13. Chin, R. L., and Hercules, D. M., *J. Phys. Chem.* **86,** 3079 (1982).
14. Cheng, C. P., and Schrader, G. L., *J. Catal.* **60,** 276 (1979).
15. Chung, K. S., and Massoth, F. E., *J. Catal.* **64,** 320 (1980).
16. Patterson, T. A., Carver, J. C., Leyden, D. E., and Hercules, D. M., *J. Phys. Chem.* **80,** 1700 (1976).
17. Delmon, B., "Preprint, 3rd International Conference of The Chemistry and Uses of Molybdenum, Ann Arbor, Mich. August 19–23, 1979."
18. Spitler, C. A., and Pollack, S. S., *J. Catal.* **69,** 241 (1981).
19. Electric Power Research Institute Annual Report, November 1977, Project 408-1, EPRI AF-574.
20. Chuang, T. J., Brundle, C. R., and Rice, D. W., *Surf. Sci.* **59,** 413 (1976).
21. Oku, M., and Hirokawa, K., *J. Electron Spectrosc.* **8,** 475 (1976).
22. Okamoto, Y., Nakano, H., Imanaka, J., and Teranishi, S., *Bull. Chem. Soc. Jpn.* **48,** 1163 (1975).
23. Knözinger, H., and Ratnasamy, P., *Catal. Rev.-Sci. Eng.* **17,** 31 (1978).
24. Giordano, N., Bart, J. C. J., Castellan, A., and Vaghi, A., *J. Less-Common Met.* **54,** 387 (1977).
25. Krylov, O. J., and Margolis, L. Y., *Kinet. Katal.* **11,** 358 (1970).
26. Lipsch, J. M. J. G., and Schuit, G. C. A., *J. Catal.* **15,** 174 (1969).
27. Topsoe, N., *J. Catal.* **64,** 235 (1980).
28. Hair, M. L., "Infrared Spectroscopy in Surface Chemistry" Dekker, New York, 1976.
29. Peri, J. B., *J. Phys. Chem.* **69,** 220 (1965).
30. Schuit, G. C. A., and Gates, B. C., *AIChE J.* **19,** 417 (1973).
31. Hagenbach, G., Courty, P. H., and Delmon, B. J., *J. Catal.* **31,** 264 (1973).
32. Furimsky, F., and Amberg, C. H., *Canad. J. Chem.* **53,** 2542 (1975).
33. De Beer, V. H. J., Dahlmans, J. G. J., Smeets, J. G. U., *J. Catal.* **42,** 467 (1976).
34. Bertolacini, R. J., Gutberlet, L. C., Kim, D. K., Robinson, K. K., EPRI AF-574, November 1977.
35. Hindin, S. G., Englhard Industries, Catalyst Development For Coal Liquefaction Contract EX-76-C-01-2335, Annual Report, November 1977.
36. Wivel, C., Candia, R., Clausen, B. S., Mørup, S., and Topsøe, H., *J. Catal.* **68,** 453 (1981).